3D characterization of fracture systems using Terrestrial Laser Scanning: an example from the Lewisian basement of NW Scotland

Pless, J.C[1,2], McCaffrey, K.J.W.[1*], Jones, R.J.[3], Holdsworth, R.E.[1], Conway, A.[2] & Krabbendam, M.[4]

[1]*CeREES, Department of Earth Sciences, Durham University, Durham, DHE 3LE, UK*

[2]*ConocoPhillips UK Ltd, Rubislaw House, Anderson Drive, Aberdeen, AB15 6FZ, UK*

[3]*Geospatial Research Ltd, Suites 7 & 8, Harrison House, Hawthorne Terrace, Durham, DH1 4EL, UK*

[4]*British Geological Survey, West Mains Road, Edinburgh, EH9 3LA, UK*

ABSTRACT

Fractured gneiss lithologies form a basement-cored high, the Rona Ridge in the Faroe Shetland basin. Basement structures are known to play an important role in the petroleum system for the overlying giant Clair field. An onshore analogue exposure in the Lewisian Gneiss Complex at Kinlochbervie in NW Scotland provides an example of a hangingwall damage zone of a large basement-hosted normal fault. In this study, we used remote sensing (2D), outcrop line sample methods (1D) and a virtual outcrop created by terrestrial laser scanning methods (3D) to characterize spatial variations of the fracture systems. Spacing distributions from 1D line samples collected from exposures and pseudo-wells constructed through the virtual outcrop show power-law distributions. The virtual outcrop data enable us to extend the scale invariant description from 1 to 3 orders of magnitude. We developed a novel box-counting workflow to provide an assessment of 2 & 3D variations in the fracture properties. Fracture density and fractal dimension is elevated whereas the number of intersections is decreased within a 220m wide volume adjacent to the fault. We discuss how the methods and results from this study can aid the development of analogue for basement reservoirs in the offshore UK continental shelf.

* corresponding author k.j.w.mccaffrey@durham.ac.uk

Introduction

Outcrop analogues provide a valuable resource for understanding and predicting subsurface reservoir sedimentary and structural properties (Wheeler & Dixon, 1980; Kerans et al. 1994; Bellian et al. 2005). Naturally fractured reservoirs, defined by Nelson (1985) as those *'in which naturally occurring fractures either play or are predicted to play a significant effect on reservoir fluid flow'*, are increasingly a target for exploration and production of hydrocarbons (Aguilera, 1995). Motivation for the current study was provided by the Clair Field, located 75km west of Shetland in the Faeroe-Shetland Basin (Coney et al. 1993). The primary Clair reservoir is situated within Devonian and Carboniferous fluvial/lacustrine sediments that overlie and onlap a fault-bounded topographic basement-cored high, the Rona Ridge that is cored by Late Archaean to Early Proterozoic granodiorite/diorite/granitic gneisses and pegmatites. Both the cover and basement are fractured and well tests suggest that there are fluid pathways through the basement connecting sedimentary packages across the main ridge structure. Fracture systems within the basement may also provide significant storage space for hydrocarbons and thus could have development potential.

Fractured reservoirs are problematic to develop because of a number of geological and engineering issues. The key geological issue is the uncertainty associated with determining and predicting the fracture geometry in the reservoir. This is because wells provide sparse spatial and dimensional sampling whilst seismic attribute methods have limited resolution at common reservoir depths. Appropriate outcrop analogues provide access to more complete size and spatial information at high resolution in 1 & 2D, e.g. (Gillespie et al. 1993; Odling et al. 1999). Many outcrops, however have the potential to provide access to 3D information, and a number of studies have demonstrated the potential for Terrestrial Laser Scanning (TLS) to provide an improved description of the 3D spatial properties of fracture systems exposed in bedrock outcrops (Ahlgren & Holmlund 2003; Trinks et al 2005; Olariu et al 2008; Seers et al 2014). Here we report a recent study on a potential outcrop analogue for the basement lithologies of the Rona ridge in which we used TLS to investigate fracture attributes and how they varied spatially in the hangingwall of a nearby major normal fault.

Regional Setting

The Scottish Highlands are underlain by a patchwork of Precambrian metamorphic terranes (Woodcock & Strachan, 2000) with the Lewisian Gneiss complex (LGC) potentially separated into several different autochthonous and allochthonous terranes that differ in lithology, metamorphic grade and age (Friend and Kinny 2001; Kinny and Friend 1997; Kinny et al. 2005) (Fig. 1a). Pless (2012) following Beacom et al (2001) carried out an assessment of faulting and fracturing for the Assynt and Rhiconich terranes within the Central and Northern regions of the mainland LGC (Fig. 1b). In this paper, we focus on a particularly well exposed outcrop of Lewisian gneisses exposed at Kinlochbervie in the Rhiconich terrane that was studied in detail by Pless (2012).

The LGC has a relatively well-established structural history of ductile fabric development, folding and Scourie dyke intrusion that predates the brittle structural history that is the topic of this study (e.g. see Park et al. 2002 and references therein). Our observations largely confirm the chronology of regionally recognised fracture sets, previously established within the mainland LGC (Beacom et al. 2001; Beacom 1999; Roberts and Holdsworth 1999) and references therein). The main fault and fracture trends in the Rhiconich terrain are NE-SW, NW-SE and N-S (Fig. 1b). In terms of age, onshore faults and fractures can be separated into four main sets:-1) cataclastic largely foliation-parallel NW-SE trending ‘Late Laxfordian’ faults (Palaeoproterozoic), 2) haematite-bearing Stoer or Torridon Group age(s) (late Mesoproterozoic; early Neoproterozoic); 3) post-Torridonian Faults (Palaeozoic) and 4) incohesive Mesozoic or younger faults (Fig. 2).

Kinlochbervie

Kinlochbervie, in the Rhiconich Terrane (NC 2296 5621), was chosen as a suitable location for this study for several reasons. From a Clair analogue perspective, the exposure sits in the hanging wall of the steeply NE-dipping Loch Inchard fault, a large, NW-SE trending normal fault (Fig. 1a). This structural setting is similar to regions within the Clair field basement, both in terms of orientation and style of fracturing observed in basement cores (see Pless 2012 for further details). The site at Kinlochbervie was also chosen because it is exposed on a hill between two lochs, hence it may be examined from almost a 360° range of viewing angles and thus provides potential access to a 3D dataset (Fig. 3).

Aerial photograph interpretation at a 1:5,000 scale (Fig. 3) enabled the identification of two main fracture lineament trends: NW-SE and NE-SW. Fieldwork shows that these represent synthetic and antithetic structures to the main Loch Inchard fault, respectively. A smaller number of N-S trending lineaments were also interpreted from the aerial photographs. Field observations suggest that the majority of fractures at Kinlochbervie are likely to be post-Torridonian structures and that they should be identifiable on the TLS dataset based on their distinctive red, hematite±carbonate mineralization and red staining. This mineralization reflects near surface fracture-hosted fluid flow and is likely sourced from the originally overlying Torridonian red beds which are presently exposed 2 km to the north of the studied outcrop (Fig. 1). This distinctive fracture set can be clearly distinguished from late joint systems and that are clearly not mineralized and are likely to be related to the most recent exhumation. The aerial photograph interpretation also suggests that the fracture density associated with the Kinlochbervie outcrop is higher compared with other areas within the Rhiconich Terrane located away from large faults or other structures (see Pless 2012).

Methods

Standard 1 & 2 D line sampling

Fracture attribute data were sampled systematically to enable comparison with other outcrops and Clair basement recovered in drill core. Fracture attributes were collected using conventional field methods along 1-D line samples (also known as scan lines, traverses or transects). Attribute data collected included orientation, spacing, aperture (width), length, host rock lithology, fault rock lithology, slickenlines, displacement and cross-cutting relationships.

3D sampling

TLS data were collected in the form of point clouds acquired using a Riegl LMS-Z420i laser scanner (Fig. 4a). The scanner uses a continuously oscillating mirror to send a laser beam to the outcrop surface and then measures the returning light. The time taken for the laser beam to leave the scanner and return (‘time of flight’) enables a the range to the target to be determined (Fig. 4b). This calculation is made for a regular grid of points across the surface at an acquisition rate of up to 12,000 points/s, creating a point cloud that defines the shape of the measured surface (Fig. 4b). Each data point in the cloud can be coloured from photographs taken using a

precisely-calibrated Nikon D100 digital SLR camera precision-mounted on top of the scanner (Fig. 4a). For more information on the scanner used and data processing methodologies, see (Kokkalas et al. 2007; Buckley et al. 2008; McCaffrey et al. 2008 and Hodgetts 2013).

Point clouds are acquired by the scanner at a series of pre-selected scan-points to give best coverage around the outcrop (Fig. 4c). A series of reference reflectors are placed around the outcrop and used to co-locate the scans in the scanner software (RiSCAN Pro v1.2.1b9). A precise location for these reflectors is generated using a differential GNSS (Global Navigation Satellite System) with sub-centimeter precision coordinates, and this is used to orientate and locate the point clouds relative to the coordinate system being used (in this case British National Grid). TLS produces a '2.5' dimensional dataset, i.e. it captures a 2-dimensional surface with the small-scale topography of the outcrop in a 3-dimensional space (Jones et al. 2008). By virtue of the high spatial resolution (typically 1 point per 3-5 cm^2) these point clouds form a high resolution virtual outcrop (c.f. McCaffrey et al. 2005) on which structural and other interpretations may be made. In this study, we 'picked' fault and fractures sets on the merged colour point cloud. Figure 4d shows an image of the Kinlochbervie coloured point cloud that formed the basis for the fracture interpretation. Detailed descriptions of TLS data acquisition and interpretation techniques are given in (Ahlgren and Holmlund 2003; Bellian et al. 2005; Hodgetts 2013; Kokkalas et al. 2007; McCaffrey et al. 2008; Olariu et al. 2008; Wilson et al. 2011).

3-dimensional fracture network model construction

The fractures have visible surface expressions, which mean that their orientations can be reconstructed by interpretation of the TLS data. The high-resolution nature of the TLS data makes it possible to interpret many of the fractures and faults visible to the naked eye at the outcrops with the advantage that parts of the outcrop that cannot be reached in the field (e.g. in otherwise inaccessible cliff sections) may also be included in the dataset (Fig. 5a). Although the resulting models occupy part of a 3D volume, the fractures may only be extrapolated into 3-dimensions with significant assumptions about their size and lateral extent. In this study, the fracture dimensions were used directly as interpreted from the point clouds without extending them into the rock mass.

Due to the nature (and resolution) of the TLS dataset, it is not possible to pick every single fracture present within each outcrop. Fractures that are manifest on the

outcrop surface as simple linear traces without topographic expression are typically not interpreted from the TLS dataset because of the uncertainty in their 3D geometry. This will clearly bias the TLS dataset as not every fracture present in the outcrop is included in the analysis. Field observations suggest that the majority of such linear fracture traces (~80%) also have short lengths (<30cm) and therefore do not contribute greatly to the overall connected fracture network. We used this observation to impose a resolution limit of >50cm fracture length. Therefore fractures with lengths less than this have been omitted from the TLS datasets.

Interpreting and creating 3D fracture planes

Fractures were interpreted by picking polylines in a circular or zigzag pattern so that as much of the visible fracture surface as possible was included (Figure 5b). The interpretation was carried out directly on the point clouds, but field photograph montages of the scanned sections were also used to confirm the extent and geometry of small-scale, less obvious fractures. The resulting set of polylines for each outcrop can then be converted into fracture planes using a plane-fitting algorithm based on a standard 3D regression. The best-fit plane is defined in terms of three perpendicular axes, where A1 = the long axis, A2 = the short axis, and A3 representing the residual error perpendicular to the plane (i.e. A1 > A2 > A3). For the orientation of the plane to be well constrained, A1 should be large, and A3 should be very small. A2 should be >> A3, and needs to be large compared with the spatial precision of the data. Any fracture planes that do not meet these criteria are re-examined, and either revised (if they were picked incorrectly) or rejected due to their unreliable planar fit. This ensures that the fracture planes used in the TLS models represent real fracture planes (both in orientation and size) as accurately as possible. The resultant fracture planes were then directly imported into the geomodelling package GOCAD™ and visualised along with a low resolution point cloud (Fig. 5c, d). More than 1500 fractures have been interpreted in the three cliff sections (e.g. Fig. 5e) and define a 3D fracture model, albeit with limited 3rd dimensional depth.

The Kinlochbervie digital outcrop was split into ‘front cliff’, ‘back cliff’ and ‘main cliff’ to make the analysis method more straightforward (Fig. 3). Because each of these cliff-sections are located in different orientation with respect to the Loch Inchard fault,

each cliff section has been treated as a separate entity for the purposes of the subsequent analyses.

Analysing the fracture networks

To allow direct comparison between the TLS and outcrop data, equivalent statistical analysis techniques have been applied to both datasets. The first of these involves the creation of 'pseudo-wells' along the scanned outcrop topographic surface, which mimic the collection of 1D line samples across the datasets (Figure 6a). Pseudo wells can then be analysed for standard fracture size, number and spatial (density/intensity) attributes in the same way as outcrop derived datasets. Datasets were not corrected for orientation bias to enable analysis in direction parallel to and perpendicular to the Loch Inchard fault. After they been corrected for orientation bias (e.g. Terzaghi method) these 1D line samples would be useful for direct comparison with sub-surface datasets from the Clair basement, where the only direct fracture observations comes from limited basement core samples.

In addition to the 1D analysis, the 3D fracture model permits a volumetric analysis of fractures. A workflow has been developed to analyse the spatial variation in the fracturing across the virtual outcrops. We utilized the SGrid functionality in GOCAD™ whereby a volume that encloses the entire outcrop is divided into blocks (cells) of a given edge length. Three different resolution SGrids were created (very low-resolution 20 x 20 x 20 cells; low-resolution 50 x 50 x 50 cells; high-resolution 300 x 150 x 100 cells – the size of each cell varies depending on the size of the outcrop (for Kinlochbervie – this was 250, 150 & 30m respectively). To determine the spatial distribution of the fractures, the cells in the SGrid that were intersected by a) the outcrop surface and, b) one or more fracture(s) were identified and grouped into arbitrary cell regions (Fig. 6b). The relative proportions of cells containing fractures versus cells without fractures gives information on the spatial properties of the fracture network. The SGrid, as explained below, provides a way of capturing 3D information on fracture distributions, but it can also be subsampled in 2D by taking slices through the 3D volume in appropriate directions (Fig. 6c, d). This allows

anisotropic properties of a fracture system to be determined by taking perpendicular slices through the volume.

We analysed the fracture distribution with a simple cell counting workflow that is directly analogous to 'box counting' methods (Gillespie et al. 1993) (Fig 6d). The number of cells containing one or more fractures is calculated as a ratio of the number of cells that the virtual outcrop surface occupies. For example if half of the cells in the SGrid that the outcrop surface intersects contain a fracture, then the ratio is 0.5. This ratio of fracture-filled cells to outcrop-filled cell is then multiplied by the total number of cells in the entire volume. Thus the well-constrained fracture network derived from the outcrop surface is used as an estimator for how fractures would fill the volume assuming that the fracture ratio remains constant in the 3rd dimension away from the scanned outcrop surface. The advantage of this approach is that it eliminates the effect that the 2.5D outcrop shape has on the fracture spatial attributes, therefore allowing outcrops of varying 2.5D geometry to be compared. Here, we illustrate this concept by using the method to illustrate how fracturing varies spatially at Kinlochbervie in relation to the Loch Inchard fault. Since the outcrop has been sampled at 3 different spatial resolutions (the 3 SGrid cell sizes), we also illustrate here how the method can be used as an assessment of the scaling properties of the system. A fractal dimension can easily be obtained by plotting log cell size (m) versus log number of cells with one or more fractures. The slope of a straight line through the values obtained from the 3 different scales is the fractal dimension of the system. This fractal dimension (D_2 or D_3) value provides a description of how area- (or volume-) filling the fractures are. For the 2D slices $1 < D_2 < 2$; whereby for $D_2 = 2$, fractures fill the entire slice whilst if D_2 approaches 1 the fractures are less area filling. In 3D, $2<D_3<3$, with $D_3 = 3$ representing fractures that fill the entire volume.

Another important fracture attribute that can be analysed using the TLS datasets is the fracture intersection distribution. The number of intersections can be taken as a proxy for fracture connectivity (e.g. Odling et al. 1999) – an important attribute for estimating fracture network permeability. In GOCAD, the intersection curves between adjoining fracture planes are calculated (Figure 5f). The intersection data may then be extrapolated throughout the 3D volume in the same way as the fracture presence data.

From 1D fieldwork analysis and outcrop pseudo-well analysis (results below) it is known that fractures within the outcrops chosen for TLS analysis exhibit power-law

distributions and exhibit scale-invariant fracture spacing. The occurrence of these scale invariant fracture sets in the outcrop fracture network models gives confidence that the 2D and 3D fractal dimension values calculated from the box-counting method provide a realistic representation of both the fracture presence and fracture intersection relationships across the modeled outcrops.

Results

Orientation analysis

At Kinlochbervie, orientation data are comparable in fieldwork, remotely sensed and TLS datasets (Figure 6a). All three datasets show fracture orientations that trend NE-SW and N-S with a subordinate NW-SE trending fracture set also present. Across the Rhiconich Terrane, NW-SE trending fault lineaments also form a prominent trend whereas at Kinlochbervie this trend is subdued. The presence of similarly orientated steeply dipping fractures in the fieldwork, TLS and aerial photo datasets and the assumed steeply dipping to sub-vertical dip of the regional fault lineaments (they are typically straight features on the DEM maps) across the Rhiconich Terrane (see Figure 4) suggests that the orientation information of fracture sets present across the Kinlochbervie area is scalable from <1m up to several kilometres.

Conventional 1D outcrop spatial analysis

The 1D line samples from Kinlochbervie (7 sample lines) consistently display power-law distributions for fracture spacing when displayed on population distribution plots (Fig. 7a). Generally, the straight line section of each dataset (on a log-log plot) fits a power-law trend line well, with R^2 values between 0.94 and 0.99 (Table 1). The slope D-value ranges from 1.05-2.17, coefficient of variation (C_v) varies between 0.78 and 1.16 and 1D fracture density varies from 2.04 - 4.06 m^{-1}. The data range between 0.1 and 1m.

TLS pseudo-well (1D) analysis.

1D line samples collected in the form of pseudo-wells were taken along strike and up/down the surface of the digital outcrops (Fig. 7b). Each fracture encountered by the pseudo-well is recorded as a distance value and from this fracture spacing (density) values have been calculated. The resulting spacing data have then been used to produce population distribution plots (Fig. 7c) and other spatial attributes – were calculated (see Table 1).

The population distribution plots from the pseudo-wells (Fig. 7c) also show consistent power-law relationships for fracture spacing across Kinlochbervie. All of the spacing samples from the TLS datasets are best described by power-law trend lines with R^2 values between 0.88 and 0.99 (Table 1). These power-law relationships have spacing values which range between 1 and 10 metres (Fig. 7c). The majority of the power-law relationships extend over more than one order of magnitude, but there are large variations in the sample D-values which vary from 0.23 to 1.57 respectively (Table 1) which may reflect the relatively low sample numbers in these datasets. The C_V for all of the pseudo- well samples collected from the TLS dataset varies between 0.82 and 1.91. Fracture density values across the TLS datasets vary between 0.07 and 0.61 m^{-1}.

2D/3D SGrid (box counting) analysis

Results from the box counting analysis are shown in Table 2. At the 30m block scale, the ratio of fractures-filled cells to outcrop-filled cells varies between 0.05 to 3.6% (Fig 8a). By analyzing the 3 parts of the model (front, back and & main cliffs) separately, we can see spatial variations in density attributes relative to the Loch Inchard fault. The NW-SE front cliff section, which is orientated parallel to and is located closest to the fault exhibits relatively constant fracture density values (c. 2% of rock volume fractured) across the model. The back cliff, which is parallel to the front cliff but further away, shows relatively low densities (0.5%) along most of its length increasing to 2.5 % at its western end. The NE-SW main cliff which is oriented approximately perpendicular to the fault shows an overall eastwards decline in density away from the fault from > 2% to < 0.5%.

Fractal dimensions were calculated for 2D slices through each of the 3 cliff face models. The main cliff shows some variation around an average D_2 value of 1.61. with peak D_2 values that appear to coincide with larger exposed cliff surfaces in the outcrop (Fig. 8b). Lower than average fracture presence D_2 values occur where the outcrop is more eroded and obscured by vegetation. The front cliff SGrid model exhibits a small decrease in D_2 values moving west to east across the cliff section (Fig. 8b). D_2 values decrease by approximately 0.55 away from the Loch Inchard Fault from the west to the east side along the outcrop (1.75 to 1.20) over a distance equivalent to 140m. The west to east decreasing fractal dimension trend is also present in the back cliff section at its extreme eastern end. Most of this section both

displays relatively low D_2 (~1.0) values suggesting an outcrop that is largely unfractured (Fig. 8b).

The single fractal dimension D_3 value for each of the models shows a similar picture with the main cliff value being significantly higher (2.72) than the other 2 cliff sections that have lower D_3 values (2.11 and 2.07). The high value for the main cliff supports the idea that a significant part of the cliff section preserved nearest to the fault is highly fractured.

Fracture intersection analysis

Fracture intersection results at Kinlochbervie vary across the three outcrop cliff sections (Fig. 8c). The average D_2 values for all three cliff sections are <1 with the average D_2 values for the front cliff section the highest calculated from the Kinlochbervie models (Fig. 8c). Fracture intersection modelling of the main cliff section yields extremely low D_2 values that are between 0.1 and 0.56 and an average D_2 value of 0.26. Similar to the fracture presence modelling, the back cliff section exhibits low D_2 values for fracture intersections with an average of 0.46. Three dimensional fracture intersection modelling at Kinlochbervie produces D_3 values that are consistently <2 (Table 2). The front cliff section exhibits the highest D_3 value (1.95, Table 2) with the main cliff section showing the lowest D_3 value (1.6, Table 2).

Discussion of spatial analysis

1D fracture analysis

Fracture spacing analyses results from outcrop and pseudo-well line samples have provided quantitative data on the 1D spatial characteristics of the fracture sets at Kinlochbervie. Thousands of individual fractures were interpreted in the TLS dataset to provide a detailed 3D model of the fracture network. These fracture network models have been analysed to provide a new understanding of the 3D fracture spatial attributes. TLS data from large outcrops such as Kinlochbervie enable fracture attributes to be collected at hectometre scales. This scale range is useful in assessing scaling of fracture attributes as it fills a gap between detailed outcrop-scale (tens of metre scales) and remotely sensed-scale observations (100s metres to km-scale analysis).

Consistent power-law relationships have emerged as being the best descriptor for the spacing distribution plots for both the Kinlochbervie outcrop and the TLS model datasets. Power-law relationships suggest scale-invariant properties to the fractures distribution. The scale range of the analysis is limited to 1 order of magnitude for the outcrop dataset (often considered to be a minimum requirement for acceptance of a power-law relationship) whereas the TLS data, despite having lower resolution, spans nearly two orders of magnitude. Thus scale-invariant behavior up to 50m in fracture spacing is much more robustly supported by using TLS in addition to conventional 1D outcrop methods.

The 1D exponent values which are an indication of how the spacing values forming the power- law relationships are weighted (i.e. ratio of small to large fracture spaces, e.g. (Pickering et al. 1995), vary widely across all TLS datasets. Due to the nature of the TLS datasets, the majority of pseudo-wells contain a small number of fracture data points in comparison to the length of the sample line. Most commonly the D-values are <1 indicating that the fracture distributions are dominated by smaller spaces, i.e. clustered. D-values also provide an indication of how clustered the data are with these common low D-values representing tight clusters (or large fracture separations) in the fracture spacing data (Gillespie et al. 1993). There are a few pseudo-wells, however, which have D- values >1 (15%), indicating that their power-law relationships are dominated by fractures that are closely spaced. C_V values are commonly >1 which suggests that the fracture sets are clustered (Gillespie et al. 1993) and supports the power-law spacing relationships. Further investigation is required to assess whether the spacing distribution exponent change with scale is a result of sampling issues or is a systematic variation (self affine variation) that could be used predictively.

Fracture density analyses conducted for the TLS pseudo-well samples yield results that are consistently lower than the outcrop samples, which is likely due to the limitations imposed by interpretation of fractures in the TLS network model rather than a reflection of the true fracture density present at each of the three key outcrops. This is because only fractures that exhibit a visible surface expression and are over 50cm in length are interpreted from TLS virtual outcrops. This means that any fractures that only present themselves as linear surface traces in the outcrop are disregarded from the TLS fracture networks, thus reducing the fracture density values for each outcrop. This lower limit threshold to the fracture lengths which are picked from the TLS datasets means that reduced fracture numbers can mostly be accounted for by the scale of the dataset. It is possible, however, that a small number

(<10%) of the fractures visible at outcrop that are longer than 50cm have not been interpreted because they are poorly defined and therefore do not have a visible fracture surface that can be picked within the TLS dataset. Thus whilst the 1D analysis from the TLS datasets extends the information to larger scales compared to the fieldwork analyses, it does not use the outcrop models to their full potential.

2 & 3D fracture analysis from TLS data

The fracture spatial analysis of the TLS datasets from Kinlochbervie has shown that the proportion of fractures present varies spatially with respect to the Loch Inchard fault. Kinlochbervie exhibits relatively high fracture densities and higher D_2 and D_3 values across the main cliff section. These higher density values are expected as Kinlochbervie sits in the hanging wall, and damage zone, of the large NW-SE trending Loch Inchard Fault. The TLS data provides a quantitative understanding of how fracture networks associated with the mainland LGC have different fracture spatial attributes, in both 2- and 3-dimensions, depending on the structural setting.

The main cliff section lies closest to the main Loch Inchard Fault plane, the higher D_2 value (than both the front and back cliff sections) supports the hypothesis that the Kinlochbervie fracture presence models record the effect that the Loch Inchard Fault has on the surrounding fracture attributes. This effect is represented by increased density close to the main fault plane and decreasing density away from this main fault back down to background fracture presence levels. From this trend, it is estimated that the damage zone of the Loch Inchard fault extends ~220m to the east of the main fault plane; with fracture density values returning to background levels (estimated from fieldwork observations) beyond this distance (Fig. 9).

At Kinlochbervie, fracture intersection density values are highest across the NW-SE front and back cliff sections. Low D_2 values represent fracture networks that are poorly intersected. D_3 fracture intersection values for Kinlochbervie show similar relationships, with the NE-SW main cliff section producing the lowest D_3 values. The simplest explanation is that the higher density/lower intersections on the main cliff reflect the prominent fracture trends across the Kinlochbervie outcrop. The main fracture trends are NE-SW and N-S which are likely to be small-scale conjugate structures to the main Loch Inchard Fault. This strong NE-SW (and sub-ordinate N-S) alignment of fractures within the Kinlochbervie TLS fracture model is responsible for the low fracture connectivity as the sub-parallel nature of the majority of the fractures means that there are fewer fracture intersections.

Fluid flow and the Clair reservoir

The creation of outcrop models for the mainland LGC provides important (and useful) quantitative datasets that can inform Clair basement predictive fracture models. The TLS analysis results have important implications for the understanding the characteristics of fracture systems in the Clair field basement. Provided the analogue is a valid one, fracture attribute values gained from outcrops and virtual outcrops provide a guide to parametrising discrete fracture network models for basement reservoirs. In this case, Kinochbervie fracture attribute data improves understanding and quantifies the effect of a major (in this case) NW trending basement fault zone (Fig. 9) on fracture controlled porosity and permeability in Lewisian rocks. Similar fault zones have been postulated in the Rona Ridge basement and would be a key component of any potential Clair field basement reservoir dependent on secondary porosity and permeability created by the associated fault and fracture networks. Using this methodology, similar studies for a range of structural settings can be developed to cover the likely deterministic inputs for a fully coupled and predictive basement/cover fluid flow model. It is important to note, however, that the model presented here does not include any information on whether or not the fractures are currently open to fluid flow, however, we note that the haematite±carbonate mineralization associated with these fractures suggests that they have been in the past. In order to use these onshore outcrop analogue models in a Clair basement appraisal, their validity as an analogue must be shown through 1) similar fracture attributes and fracture fills, 2) demonstrably similar basin histories.

Conclusions

Our analysis of brittle deformation in the Lewisian basement outcrop at Kinlochbervie shows that 2 main fault and fracture sets are present (NW-SE and NE-SW). These structures preserve abundant evidence of mineralization (haematite, carbonate) suggesting that they have acted as significant permeability pathways in the geological past. The fracture spacing attributes are best described by power-law distributions over at least 3 orders of magnitude. The TLS method is able to extend the 1D sampling scale range from decametre to hectometre scales and provides access to useful 2 & 3D fracture attribute information. Spacing attributes (density) shows systematic variations in the hangingwall to the Loch Inchard Fault. The influence of the fault structure, i.e. its damage zone extends some c. 220m into the hangingwall of the basement fault. Recognition of similar trending structures within the Rona Ridge, in the basement to the Clair field mean that Kinlochbervie could act

as a potential analogue provided similar basin histories and fracture attributes can be established. In this case the fracture attribute data provide potentially important constraints on the scaling relationships and properties of fault and fractures systems that may be present in any basement reservoirs that might be associated with oilfields such as Clair.

Acknowledgements

This study resulted from a PhD studentship funded by the Clair Joint Venture which is gratefully acknowledged.

References

Aguilera, R. 1995. *Naturally fractured reservoirs*. 2nd ed. ed. PennWell, Tulsa, Okla.

Ahlgren, S. & Holmlund, J. 2003. Using 3-D Outcrop Laserscans for Fracture Analysis. *AAPG Search & Discovery article #40099*.

Beacom, L., Holdsworth, R.E., McCaffrey, K.J.W. & Anderson, T. 2001. A quantitative study of the influence of pre-existing compositional and fabric heterogenities upon fracture zone development during basement reactivation. *In*: Holdsworth, R.E., Strachan, R.A., Magloughlin, J.F. & Knipe, R.J. (eds.) *The nature and tectonic significance of fault zone weakening*. Geological Society Special Publication. 186, 195-211.

Beacom, L.E. 1999. *The Kinematic Evolution of Reactivated and Non-Reactivated Faults in Basement Rocks, NW Scotland*. Ph.D., Queen's University.

Bellian, J.A., Kerans, C. & Jennette, D.C. 2005. Digital Outcrop Models: Applications of Terrestrial Scanning Lidar Technology in Stratigraphic Modeling. *Journal of Sedimentary Research*, **75**, 166-176, doi:10.2110/jsr.2005.013.

Buckley, S.J., Howell, J.A., Enge, H.D. & Kurz, T.H. 2008. Terrestrial laser scanning: data acquisition, processing and accuracy considerations. Journal of the Geolgoical Society, London, 165, 625-638.

Coney, D., Fyfe, T.B., Retail, P. & Smith, P.J. 1993. Clair appraisal: the benefits of a co-operative approach. *In*: Parker, J.R. (ed.) *Petroleum geology of northwest Europe: Proceedings of the 4th conference*. Geological Society, London. Falt, U., Guerin, G., Retail, P. & Evans, M. 1992. Clair Discovery: Evaluation of Natural Fracturation in a Horizontal Well Drilled in the Basement and Producing From Overlying Sediments. *Eurpoean Petroleum Conference* Cannes, France, 11-21.

Friend, C.R.L. & Kinny, P. 2001. A reappraisal of the Lewisian Gneiss Complex: geochronological evidence for its tectonic assembly from disparate mterranes in the Proterozoic. *Contributions to Mineralogy and Petrology*, **142**, 198-218.

Gillespie, P.A., Howard, C.B., Walsh, J.J. & Watterson, J. 1993. Measurement and characterisation of spatial distributions of fractures. *Tectonophysics*, **226**, 113-141.

Hodgetts, D. 2013. Laser scanning and digital outcrop geology in the petroleum

industry: A review. *Marine and Petroleum Geology*, **46**, 335-354, doi:10.1016/j.marpetgeo.2013.02.014.
Jones, R.R., Wawrzyniec, T.F., Holliman, N.S., McCaffrey, K.J.W., Imber, J. & Holdsworth, R.E. 2008. Describing the dimensionality of geospatial data in the earth sciences--Recommendations for nomenclature. *Geosphere*, **4**, 354-359, doi: 10.1130/ges00158.1.
Kerans, C., Lucia, F,J. & Senger, R.K. 1994. Integrated Characterization of Carbonate Ramp Reservoirs using Permian San Andres Formation Outcrop Analogs. American Association of Petroleum Geologists, 78, 181-216.
Kinny, P.D. & Friend, C.R.L. 1997. U-Pb isotopic evidence for the accretion of different crustal blocks to form the Lewisian Complex of northwest Scotland. *Contributions to Mineralogy and Petrology*, **129**, 326-340.
Kinny, P.D., Friend, C.R.L. & Love, G.J. 2005. Proposal for a terrane-based nomenclature for the Lewisian Gneiss Complex of NW Scotland. *Journal of the Geological Society*, **162**, 175-186, doi: 10.1144/0016-764903-149.
Kokkalas, S., Jones, R.R., McCaffrey, K.J.W. & Clegg, P. 2007. Quantitative fault analysis at Arkitsa, Central Greece, using terrestrial laser-scanning (LiDAR). *Bulletin of the Geological Society of Greece*, **37**, 1-14.
McCaffrey, K.J.W., Jones, R.R., Holdsworth, R.E., Wilson, R.W., Clegg, P., Imber, J., Holliman, N. & Trinks, I. 2005. Unlocking the spatial dimension: digital technologies and the future of geoscience fieldwork. J. Geological Society of London, 161, 927-938.
McCaffrey, K.J.W., Feely, M., Hennessy, R. & Thompson, J. 2008. Visualization of folding in marble outcrops, Connemara, western Ireland: An application of virtual outcrop technology. *Geosphere*, **4**, 588-599, doi:10.1130/ges00147.1.
Nelson, R.A. 1985. *Geological analysis of naturally fractured reservoirs.* Gulf Publishing Company, Houston.
Odling, N.E., Gillespie, P., Bourgine, B., Castaing, C., Chiles, J.P., Christensen, N.P., Fillion, E., Genter, A., Olsen, C., Thrane, L., Trice, R., Aarseth, E., Walsh, J.J. & Watterson, J. 1999. Variations in fracture system geometry and their implications for fluid flow in fractures hydrocarbon reservoirs. *Petroleum Geoscience*, **5**, 373-384, doi: 10.1144/petgeo.5.4.373.
Olariu, M.I., Ferguson, J.F., Aiken, C.L.V. & Xu, X.M. 2008. Outcrop fracture characterization using terrestrial laser scanners: Deep-water Jackfork sandstone at Big Rock Quarry, Arkansas. *Geosphere*, **4**, 247-259, doi:10.1130/Ges00139.1.
Park, R.G., Stewart, A.D. & Wright, D.T. *The Hebridean Terrane*. In Trewin, N.H. (ed) The Geology of Scotland. The Geological Society of London, 576p.
Pickering, G., Bull, J.M. & Sanderson, D.J. 1995. Sampling power-law distributions. *Tectonophysics*, **248**, 1-20.
Pless, J.C. 2012. Characterising fractured basement using the Lewisian Gneiss Complex, NW Scotland [electronic resource] : implications for fracture systems in the Clair Field basement. http://etheses.dur.ac.uk/3489/.
Roberts, A.M. & Holdsworth, R.E. 1999. Linking onshore and offshore structures: Mesozoic extension in the Scottish Highlands. *Journal of the Geological Society*, **156**, 1061-1064, doi: 10.1144/gsjgs.156.6.1061.
Seers, T.D. & Hodgetts, D. 2014. Comparison of digital outcrop and conventional data collection approaches for the characterization of naturally fractured reservoir rocks. From: Spence, G.H. Redfern, J, Aguilera, R., Bevan, T.G., Cosgrove, J.W., Couples, G.D. & Daniel, J.-M. (eds) Advances in the study of Fractured Reservoirs. Geological Society, London, Special Publications, 374, 51-77.

Trinks, I., Clegg, P., McCaffrey, K.J.W., Jones, R., Hobbs, R., Holdsworth, R.E., Holliman, N.S., Imber, J., Waggott, S. & Wilson, R.W. 2005. Mapping and analysing virtual outcrops. *Visual Geosciences*, 1-7.
Wilson, C.E., Aydin, A., Karimi-Fard, M., Durlofsky, L.J., Sagy, A., Brodsky, E.E., Kreylos, O. & Kellogg, L.H. 2011. From outcrop to flow simulation: Constructing discrete fracture models from a LIDAR survey. *AAPG Bulletin*, **95**, 1883-1905, doi: Doi 10.1306/03241108148.
Wheeler, R.L. & Dixon, J.M. 1980. Intensity of systematic joints: Methods and applications. Geology, 8, 230-233.
Woodcock, N.H. & Strachan, R.A. 2000. *Geological history of Britain and Ireland*. Blackwell Science, Oxford.

Figure Captions

Figure 1. Location map for study area. a) Basement geology of NW highlands showing the Lewisian terranes major structures (shear zones and brittle faults). b) Lineament interpretation of NEXTMap digital elevation model with rose diagrams showing principal trends.

Figure 2. Fault structural styles in the Lewisian basement of NW Scotland. Inset cartoon shows interpretation of relative timing in each case. a) Late Laxfordian faults formed parallel to Canisp shear zone (Paleoproterozoic). b) Later there are Stoer Group age fractures which developed in transtension during the deposition of the Stoer Group sediments (Neoproterozoic) on top of the Lewisian. c) Sediment-infilled fault of Stoer Group age. d) Cataclasite of same age, e) Large fault (possibly Mesozoic) showing f) incohesive gouges and g) down-dip slickensides.

Figure 3. The locality at Kinlochbervie a) the location on the NW-trending Loch Inchard Fault and b) the sampled outcrop with an aerial photograph interpretation of faults and fractures (data plotted on rose diagram).

Figure 4. Terrestrial laser scanning of Kinlochbervie. a) Riegl LMS z420i scanner used to acquire the data. b) laser scanning principles (see text for explanation) c) the resultant coloured point cloud showing the scanner locations and the tie points that were used for registration. d) View of Kinlochbervie showing the main cliff face behind the B801 road. Lamp-posts (c. 5m high) along the edge of road give an impression of the scale of the model.

Figure 5. Interpretion of fractures from TLS data. a) a fracture plane visible in the virtual outcrop. b) a polyline digitized in the data as a series of zig-zag lines to capture the 3D geometry accurately. c) best-fit plane to polyline. d) same plane viewed ‘end on’. e) 3D view of Kinlochbervie model with c. 1500 planes interpreted in correct geospatial position.

Figure 6. Analysis of the Kinochbervie virtual outcrop fracture model. a) A series of pseudo-wells ‘drilled’ vertically and horizontally across the 3 outcrop faces provide 2D datasets to compare with outcrop data. The outcrop faces are shown as meshed low-resolution surface patches for reference (red - front cliff, green - main cliff, blue - back cliff. b) sequential sampling of the modeled fractures using SGrid 2D slices (pale square). The number of fractures in each slice gives a 2D density attribute and can be summed along sequential slices to give a 3D attribute. c) SGrid 2D slice intersecting fractures and the outcrop surface (red lines on square). d) SGrid slice of fracture model (delete). e) fracture plane intersections (3 shown by arrows). f) intersection lines that are sampled by the SGrid 2D slices for the connectivity attribute.

Figure 7. Results from 1D analysis of a) fractures in outcrop datasets and b) pseudo-well data derived from the TLS models. See text for discussion of results. Pseudowell locations are shown on Fig 6b.

Figure 8. Results from the 2D/3D analysis. a) fracture density variations on the 3 cliff faces in 3D perspective b) D2 fractal dimensions and varation across each cliff face. c). Number of fracture intersection variations across in the 3 cliff faces. See text for discussion of results.

Figure 9. Summary of Kinlochbervie outrcrop fracture analysis (with cartoon showing the conceptual model).

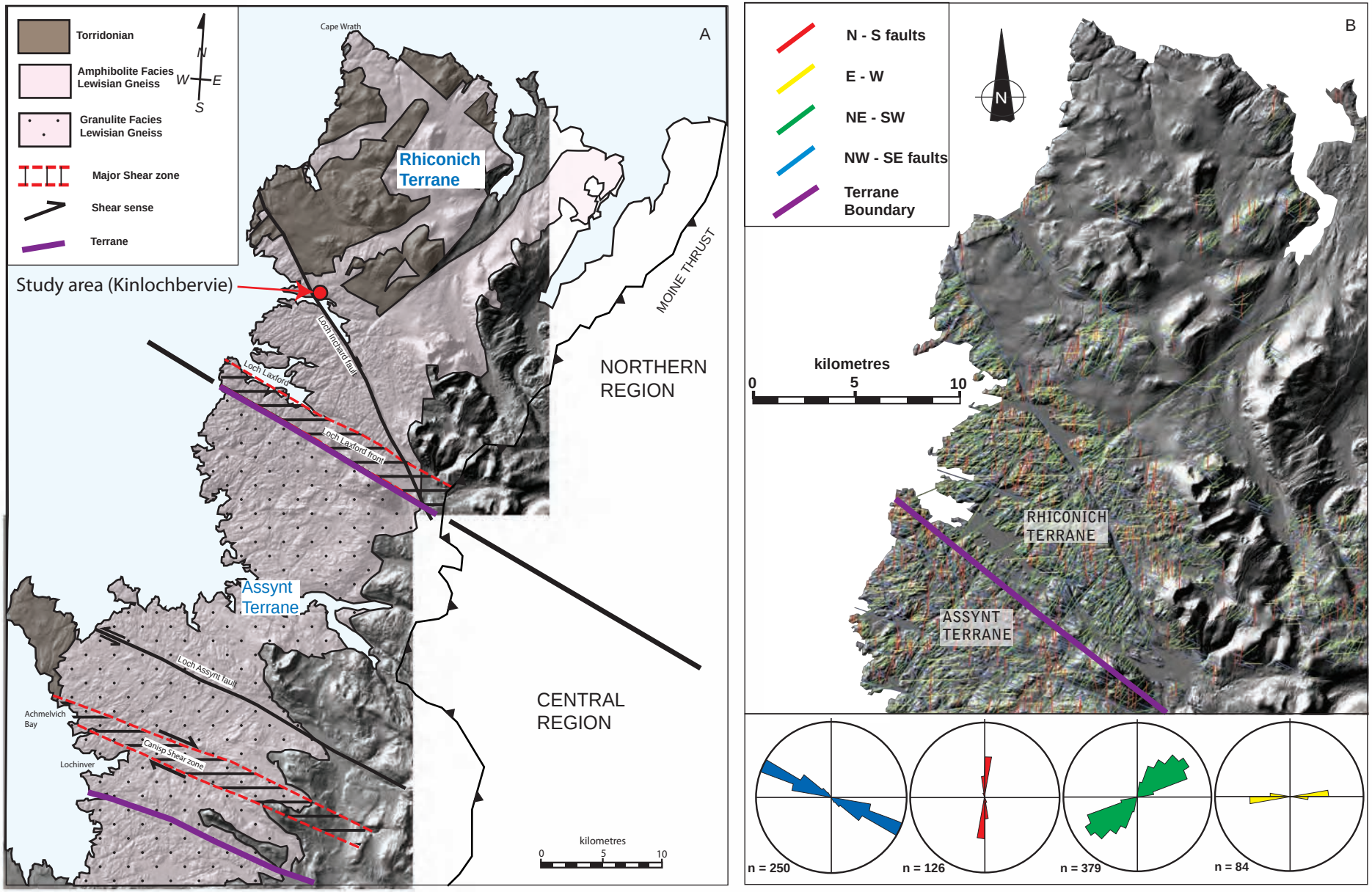
A
Torridonian
Amphibolite Facies Lewisian Gneiss
Granulite Facies Lewisian Gneiss
Major Shear zone
Shear sense
Terrane
N
W
E
S
Cape Wrath
Rhiconich Terrane
MOINE THRUST
Study area (Kinlochbervie)
Loch Inchard fault
Loch Laxford
Loch Laxford front
NORTHERN REGION
Assynt Terrane
Loch Assynt fault
Achmelvich Bay
Canisp Shear zone
Lochinver
CENTRAL REGION
kilometres
0
5
10
B
N - S faults
E - W
NE - SW
NW - SE faults
Terrane Boundary
N
kilometres
0
5
10
RHICONICH TERRANE
ASSYNT TERRANE
n = 250
n = 126
n = 379
n = 84

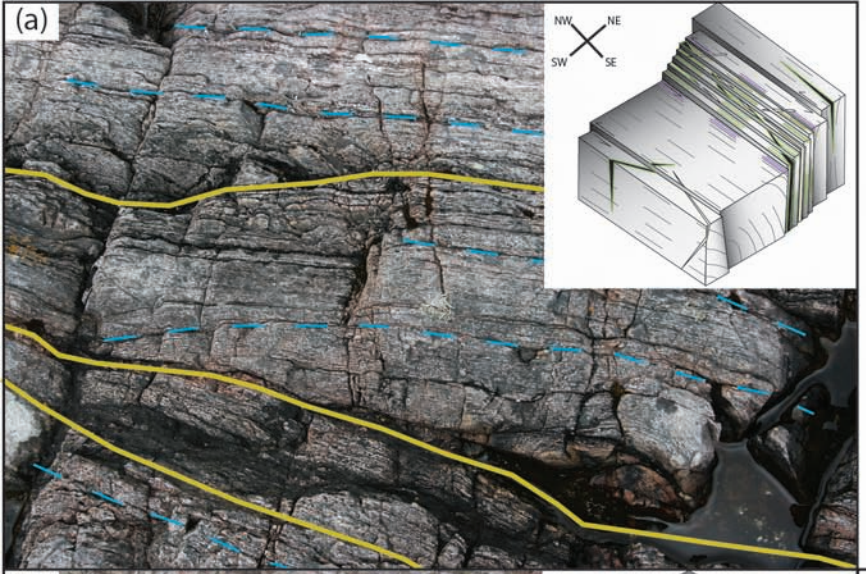
(a)
NW
NE
SW
SE

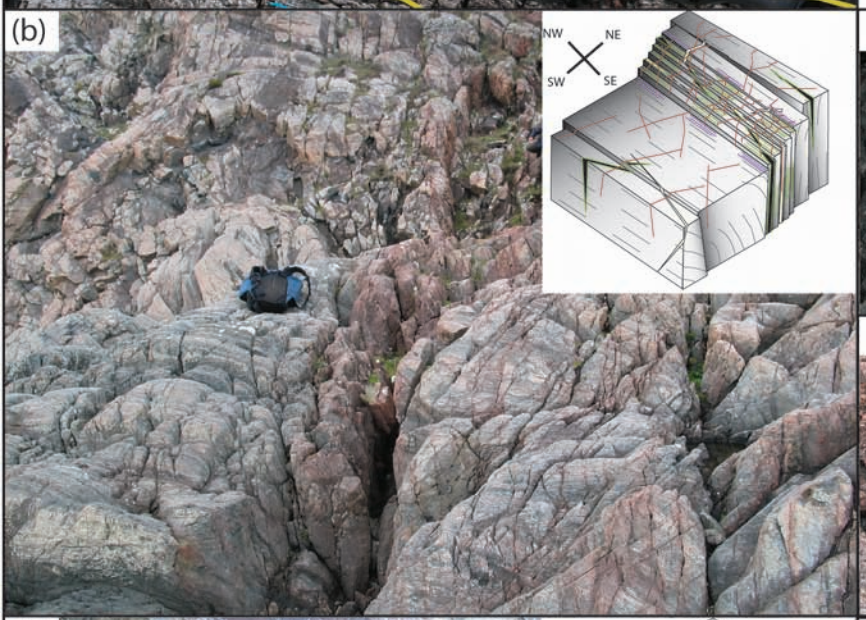
(b)
NW
NE
SW
SE


(c)


(d)

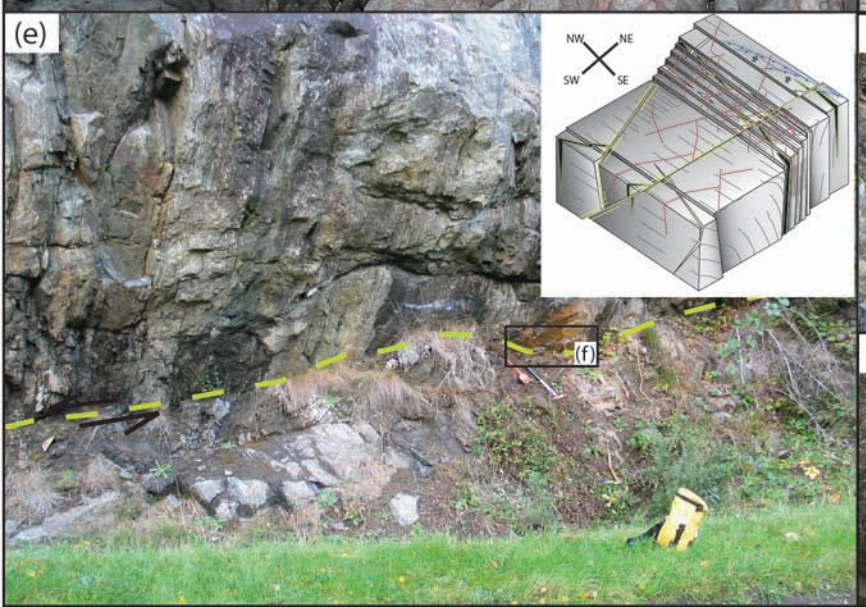
(e)
NW
NE
SW
SE
(f)


(f)
1
2


(g)

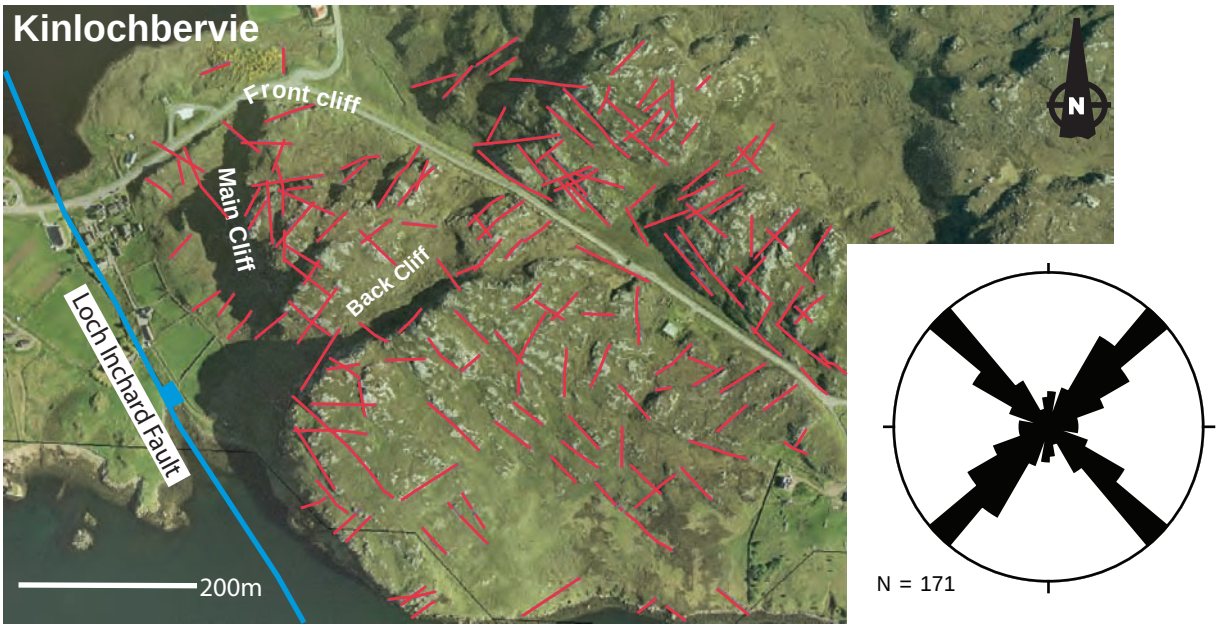
Kinlochbervie
Front cliff
Main Cliff
Back Cliff
Loch Inchard Fault
200m
N
N = 171

(a)

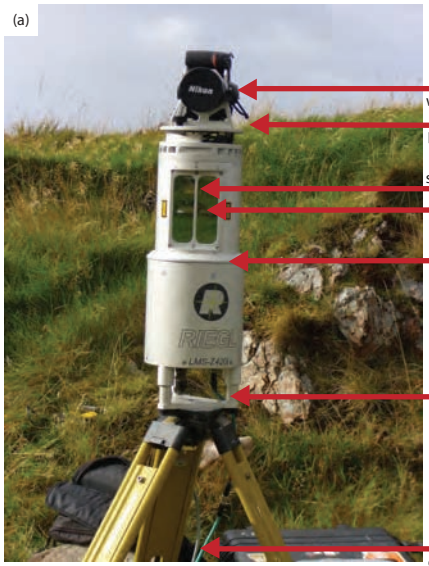

well-calibrated camera

precision camera mount

scanner window

mirrors

rotates 360°

can be levelled
or used with a tilt mount

connected to a
ruggedized laptop

(b)

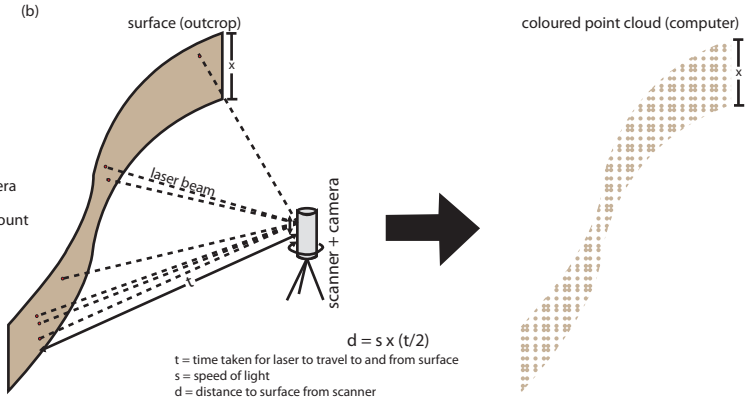

$d = s \times (t/2)$

t = time taken for laser to travel to and from surface
s = speed of light
d = distance to surface from scanner

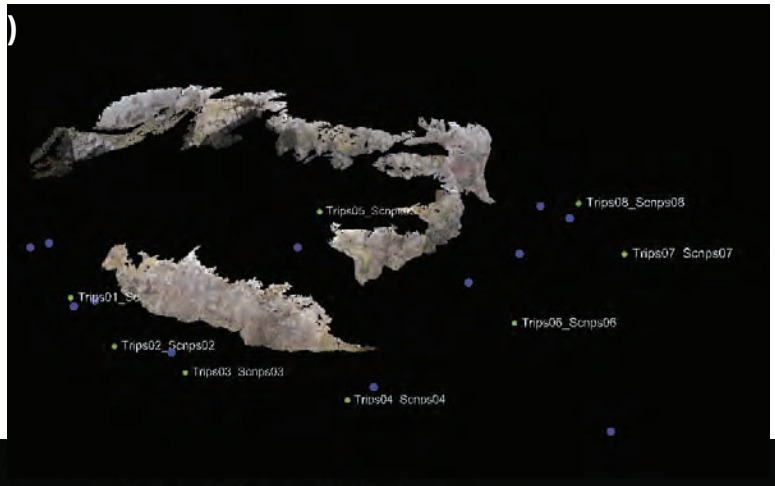

(d)

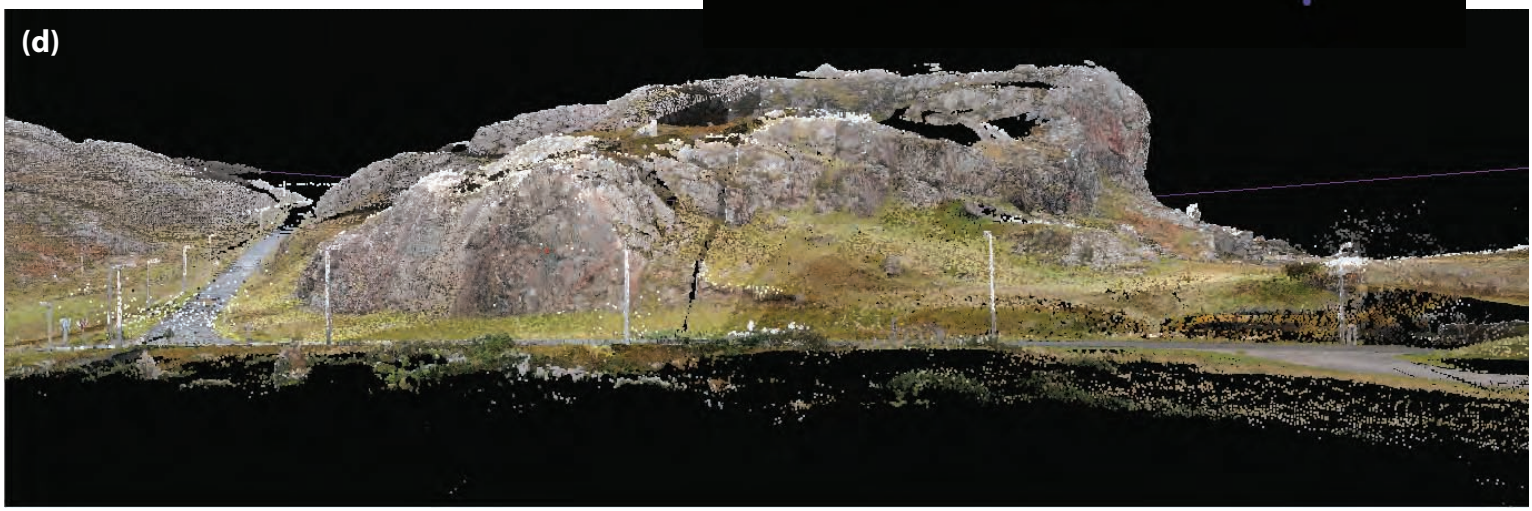

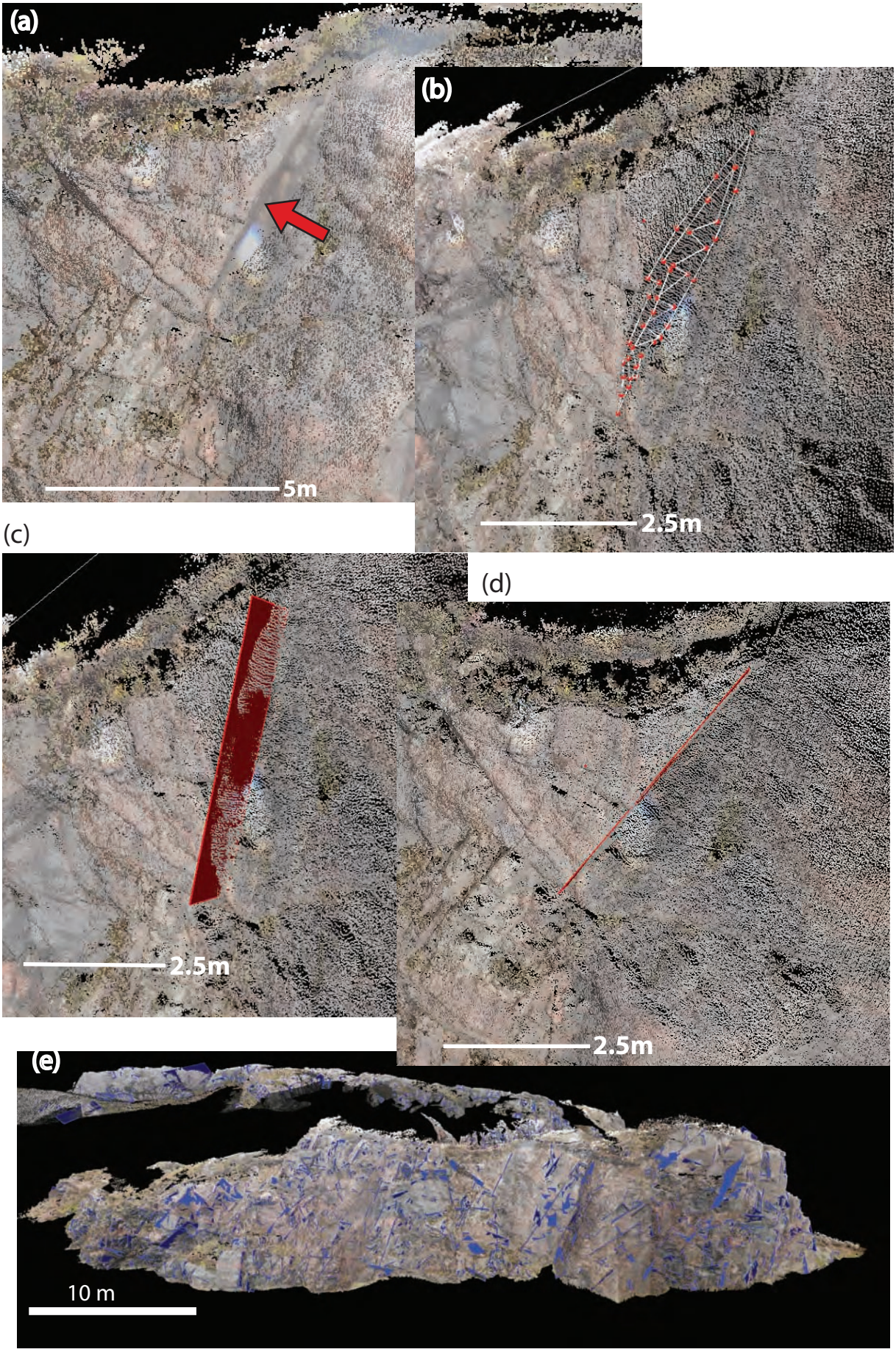
(a)
5m
(b)
2.5m
(c)
2.5m
(d)
2.5m
(e)
10 m

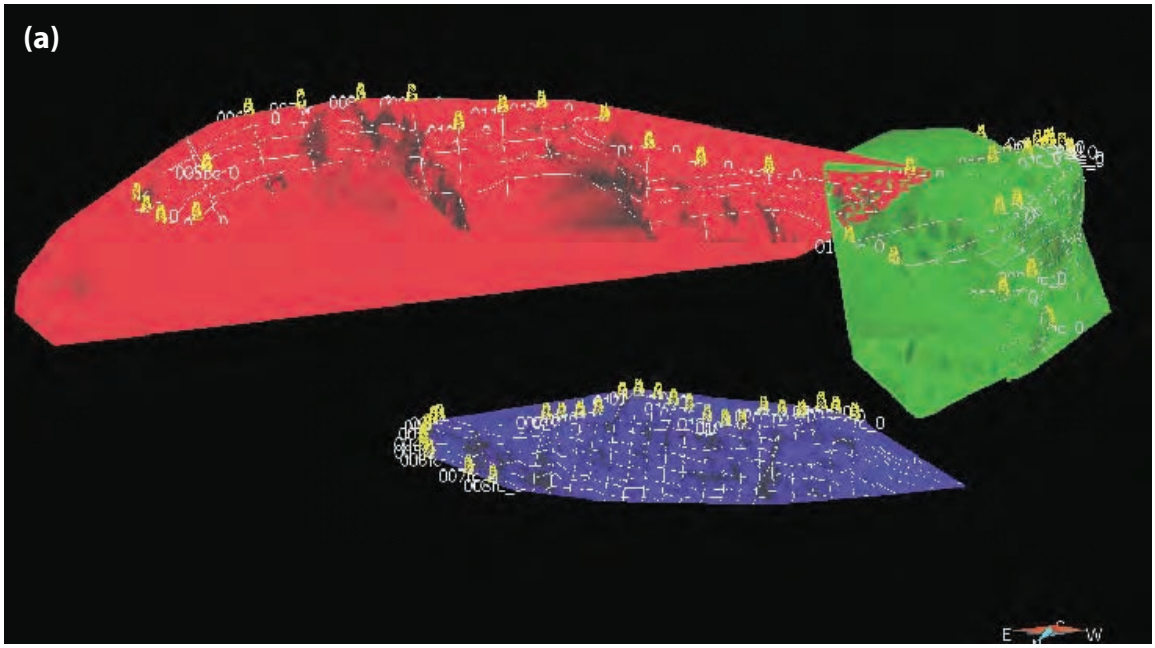
(a)
E
W

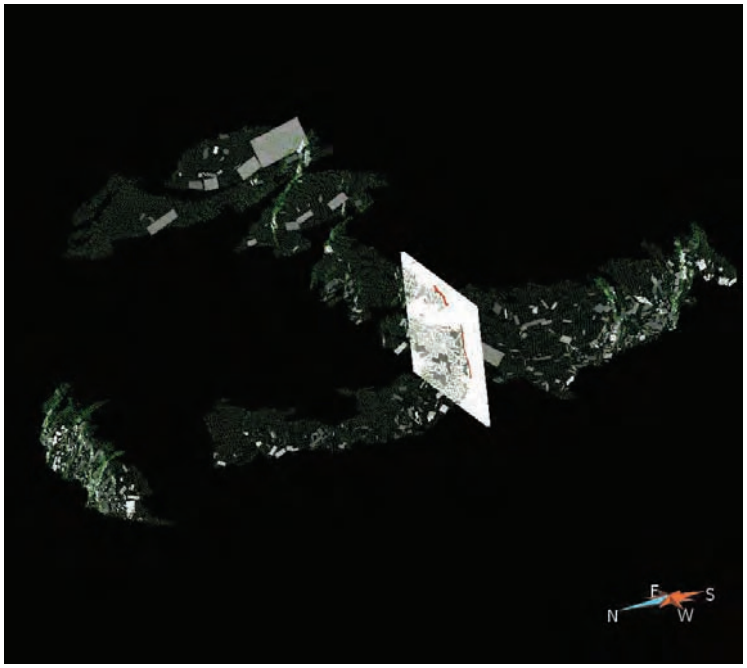
E
S
N
W

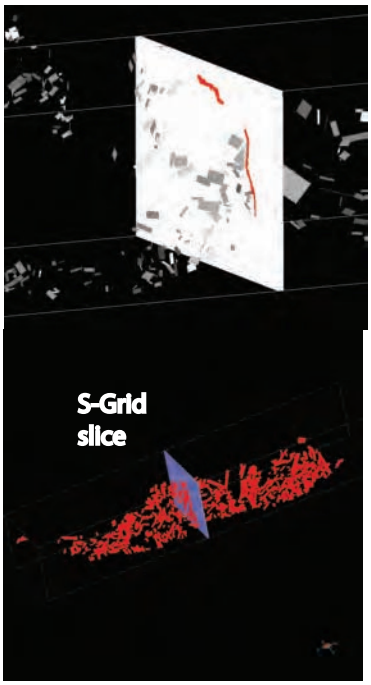
S-Grid
slice

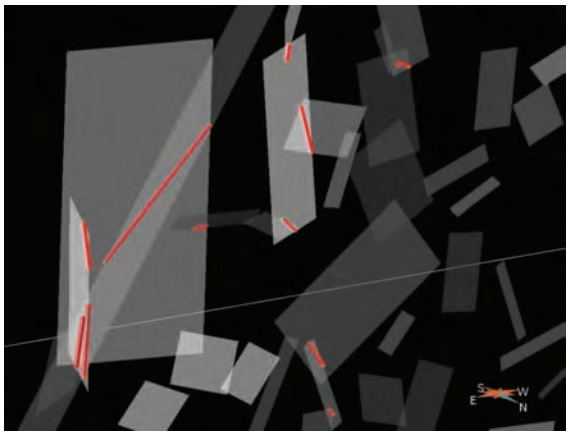

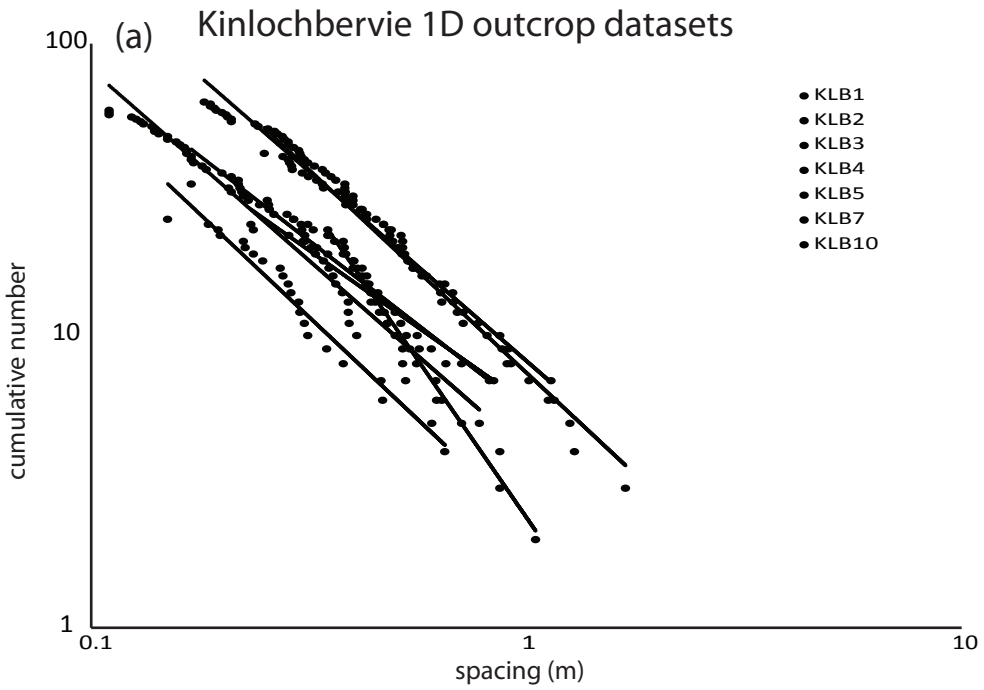
(a)
Kinlochbervie 1D outcrop datasets
100
10
1
cumulative number
0.1
1
10
spacing (m)
KLB1
KLB2
KLB3
KLB4
KLB5
KLB7
KLB10

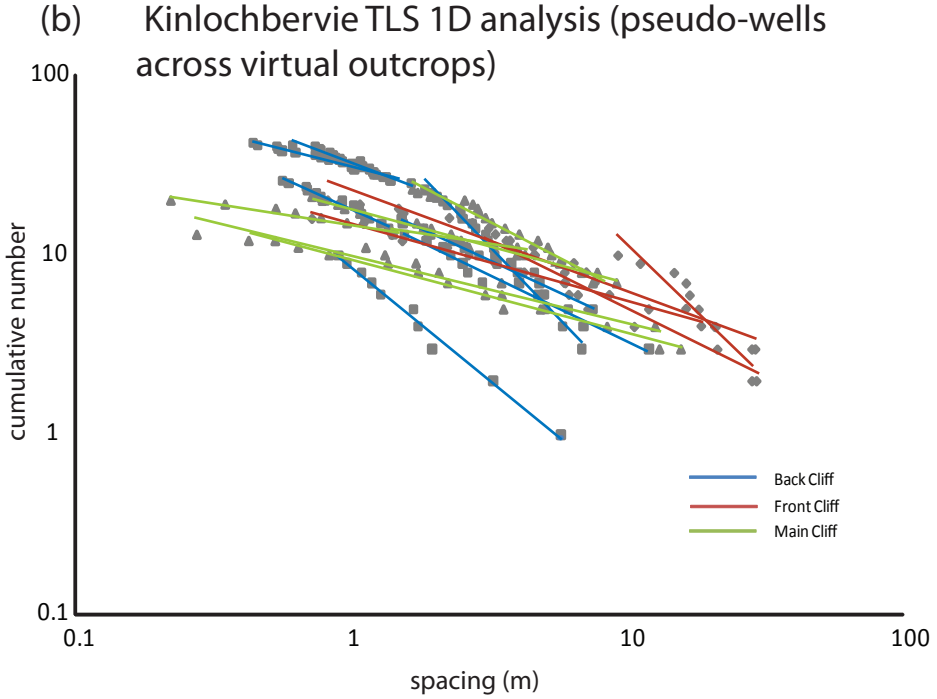
(b)
Kinlochbervie TLS 1D analysis (pseudo-wells across virtual outcrops)
100
10
1
0.1
cumulative number
0.1
1
10
100
spacing (m)
Back Cliff
Front Cliff
Main Cliff

(a)

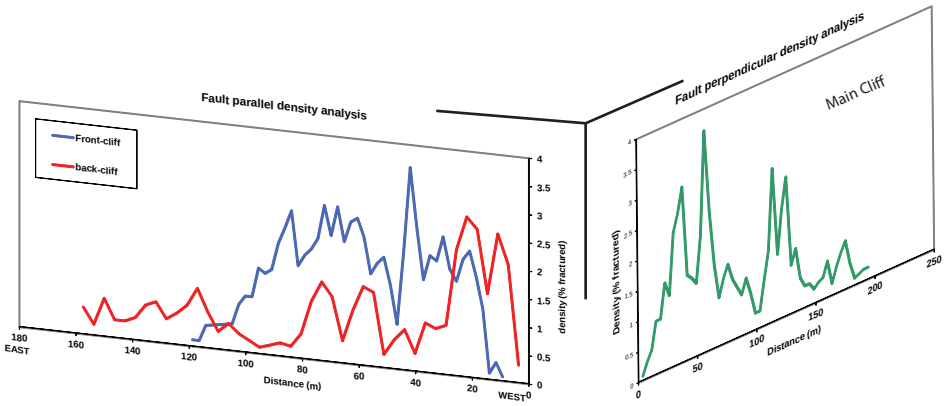
Fault parallel density analysis
Front-cliff
back-cliff
density (% fractured)
Distance (m)
EAST
WEST
Fault perpendicular density analysis
Main Cliff
Density (% fractured)
Distance (m)

(b)

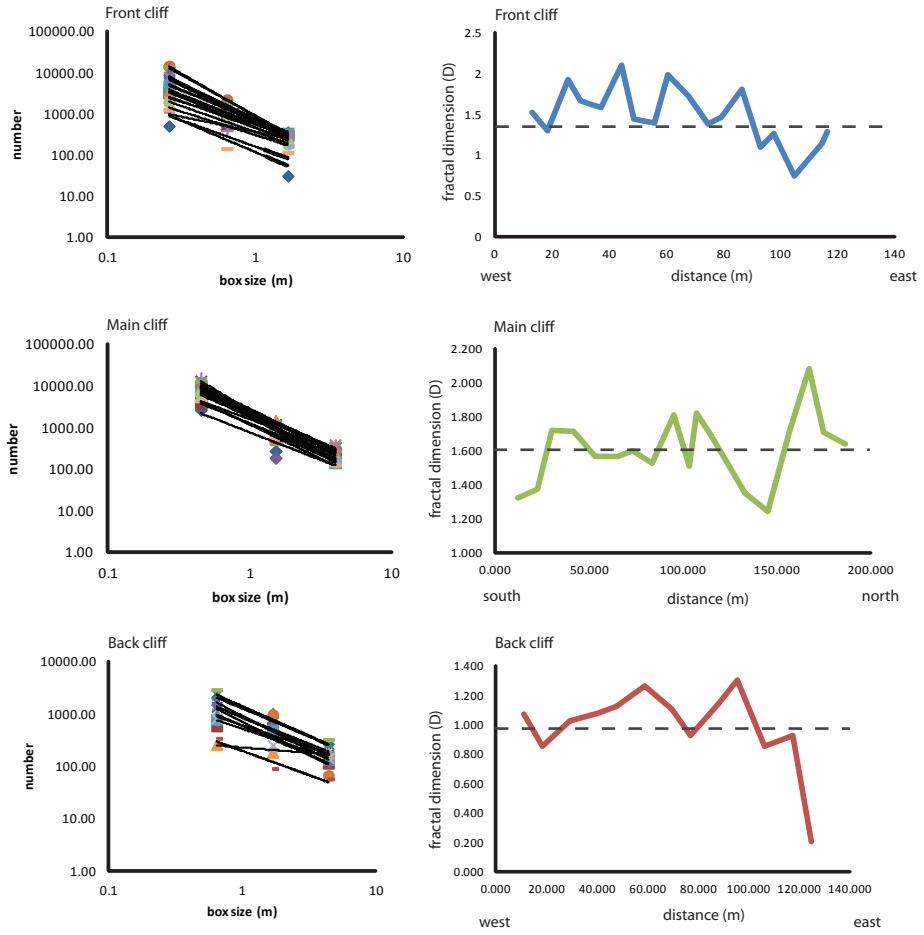
Front cliff
number
box size (m)
Front cliff
fractal dimension (D)
west
distance (m)
east
Main cliff
number
box size (m)
Main cliff
fractal dimension (D)
south
distance (m)
north
Back cliff
number
box size (m)
Back cliff
fractal dimension (D)
west
distance (m)
east

(c)

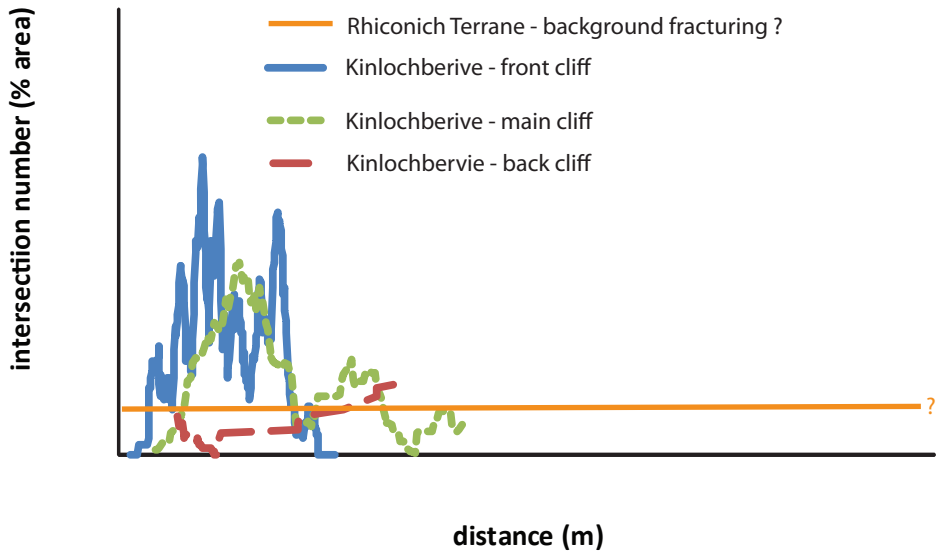
Rhiconich Terrane - background fracturing ?
Kinlochberive - front cliff
Kinlochberive - main cliff
Kinlochbervie - back cliff
intersectiion number (% area)
?
distance (m)

Kinlochbervie

Major NE-SW trending fault produced enhanced basement fracturing over a c. 220 m wide damage zone

Fracture spacing characterised by power law distribution with D1 for spacing data lower in outcrop compared to virtual outcrops
In the damage zone :-
Fracture numbers scale in 2 and 3D
with D2 = 1.36, D3 = 2.30
Fracture intersections scale in 2 and 3D
D2 = 0.51, D3 =1.74